Recognition protein C1q of innate immunity agglutinates nanodiamonds without activating complement

Agathe Bélime, Nicole M. Thielens, Edmond Gravel, Philippe Frachet, Sarah Ancelet, Pascale Tacnet-Delorme, Charlotte Caneiro, Jane Chuprin, Christine Gaboriaud, Guy Schoehn, et al.

Recognition protein C1q of innate immunity agglutinates nanodiamonds without activating complement

Agathe Belime[a], Nicole M. Thielens[b], Edmond Gravel[a], Philippe Frachet[b], Sarah Ancelet[b], Pascale Tacnet[b], Charlotte Caneiro[b], Jane Chuprin[c], Christine Gaboriaud[b], Guy Schoehn[b], Eric Doris[a], Wai Li Ling[b]

[a] Service de Chimie Bioorganique et de Marquage (SCBM), CEA, Université Paris-Saclay, 91191 Gif-sur-Yvette, France.

[b] Univ. Grenoble Alpes, CEA, CNRS, IBS, F-38000 Grenoble, France.

[c] Nano/Bio Interface Center, University of Pennsylvania, Philadelphia, PA, USA.

Research Funding

This work has been funded by the Transversal Toxicology Program of the CEA (NanoImmunoTox). This work used the platforms of the Grenoble Instruct-ERIC Centre (ISBG; UMS 3518 CNRS-CEA-UGA-EMBL) with support from FRISBI (ANR-10-INSB-05-02) and GRAL (ANR-10-LABX-49-01) within the Grenoble Partnership for Structural Biology (PSB). The IBS electron microscope facility is supported by the Rhône-Alpes Region, the *Fonds FEDER*, the *Fondation Recherche Médicale* (FRM), and the GIS-IBISA. The "*Service de Chimie Bioorganique et de Marquage*" belongs to the Laboratory of Excellence in Research on Medication and Innovative Therapeutics (ANR-10-LABX-0033-LERMIT). JC was supported by the GIANT International Internship Program (GIIP) of Grenoble.

Conflict of Interest Statement

The authors declare no conflicts of interest associated with this work.

Word count for Abstract: 150

Word count for Manuscript (Introduction, Methods, Results, and Discussion): 5023

Number of References: 49

Number of Figures: 7

Number of Tables: 1

Number of Supplementary online-only file: 1

List of Abbreviations

DLS dynamic light scattering

DMF dimethylformamide

EDTA ethylenediaminetetraacetic acid

ELISA enzyme-linked immunosorbent assay

FSC forward scatter

gC1q globular domain of C1q

HSA human serum albumin

IC immune complex

MAC membrane attack complex

MBL mannose-binding lectin

ND nanodiamond

ND-COOH oxidized nanodiamond

ND-PEG PEGylated nanodiamond

PEG polyethylene glycol

PMA phorbol 12-myristate 13-acetate

SDS-PAGE sodium dodecyl sulfate-polyacrylamide gel electrophoresis

SPR surface plasmon resonance

SSC side scatter

SST sodium silicotungstate

TBS tris-buffer-saline

TEM transmission electron microscopy

TGA thermogravimetric analysis

THF tetrahydrofuran

XPS X-ray photoelectron spectroscopy

Recognition protein C1q of innate immunity agglutinates nanodiamonds without activating complement

Agathe Belime[a], Nicole M. Thielens[b], Edmond Gravel[a], Philippe Frachet[b], Sarah Ancelet[b], Pascale Tacnet[b], Charlotte Caneiro[b], Jane Chuprin[c], Christine Gaboriaud[b], Guy Schoehn[b], Eric Doris[a], Wai Li Ling[b]

[a] Service de Chimie Bioorganique et de Marquage (SCBM), CEA, Université Paris-Saclay, 91191 Gif-sur-Yvette, France.

[b] Univ. Grenoble Alpes, CEA, CNRS, IBS, F-38000 Grenoble, France.

[c] Nano/Bio Interface Center, University of Pennsylvania, Philadelphia, PA, USA.

Abstract

Nanodiamonds are promising nanomedicines for diagnostic and therapeutic applications. As nanodiamonds are mainly administered intravenously, it is critical to understand the humoral immune response upon exposure to nanodiamonds. Here, we report the interactions of pristine, oxidized, and PEG-functionalized nanodiamonds with human complement, an important part of our humoral innate immunity. In particular, we report the nanodiamond binding properties of the recognition protein of the classical complement pathway: C1q, which also takes part in many other physiological and pathological processes. Our results show similar trends in the effects of C1q on the three types of nanodiamonds. Complement activation assays using human serum show that the nanodiamonds trigger slight activities *via* the alternative pathway and no response *via* the classical pathway. Nevertheless, surface plasmon resonance shows that C1q binds the nanodiamonds and transmission electron microscopy reveals their agglutination. Studies with macrophages further show that C1q attachment affects their phagocytosis and cytokine response.

Key words: nanodiamonds, C1q, complement, macrophage

1. Introduction

Nanodiamonds (NDs) are promising candidates for a range of biomedical applications due to their favorable physical, chemical, and biological properties.[1–3] Their potential fluorescence and ease of functionalization make them excellent candidates to combine diagnosis and therapy within the same nanoparticle.[4,5] Nanodiamonds have also been used for implant coating.[6] Moreover, NDs are known to have the greatest biocompatibility among carbon nanomaterials in terms of cytotoxicity and production of reactive oxygen species.[1,7] Interesting results in biomedical applications, especially in challenging areas such as targeted cancer therapy, prevention of Alzheimer's disease, and brain imaging, have been obtained with NDs.[8–11]

To be applied clinically, the safety of ND-based nanomedicines needs to be comprehensively evaluated. To date, toxicology studies of NDs have mainly focused on *in vivo* murine models and *in vitro* cellular toxicity.[6,7,12–16] Since many potential biomedical applications of NDs entail their contact with the humors (bodily fluids), it is important also to understand the response of the human humoral immune system towards these nanomaterials. While there have been studies involving the effect of NDs on human blood components,[17,18] studies that concern the human complement, the subject of the present work, have not been reported.

The complement system forms a crucial part of our humoral immunity and is highly species specific. Contrary to acquired immunity, complement in innate immunity reacts spontaneously against foreign objects detected in the body. Complement activation occurs through three pathways (classical, lectin, and alternative) and triggers an amplifying cascade of enzyme activation and cytokine release. The cascade terminates in the formation of a cell-

killing membrane attack complex (MAC). Inappropriate complement activation can lead to inflammation and tissue injury with detrimental consequences.[19]

Our present study focuses on the interaction of NDs with C1q, the recognition unit of the first complement protein complex C1, which initiates the classical pathway of complement. The C1 complex comprises C1q bound non-covalently to the pro-enzyme $C1r_2s_2$ tetramer. C1 activates complement in innate immunity when C1q binds to pathogens directly as well as in acquired immunity when C1q recognizes bound antibodies. The complement cascade is triggered when C1q binds to an activator, which causes a structural change that activates the pro-enzyme $C1r_2s_2$. From a structural point of view, C1q resembles a bouquet with a collagen stem branching out into six collagen arms each ending in a globular head domain (gC1q).[20] The gC1q domain binds to a range of targets through recognition of charged groups.[21] We have previously shown that gC1q also binds to graphene and carbon nanotubes.[22,23]

Apart from activating the complement in serum as a C1 complex subunit, C1q is a ubiquitous and versatile protein with many other functions, including the clearance of apoptotic cells, modulation of immune cell functions, pregnancy, and cancer control.[24,25] Importantly, C1q is involved in physiological and pathological processes in the brain, such as synaptic trimming in brain maturation and pathogenesis of neurodegenerative diseases.[26,27] Binding of C1q to administered NDs may affect the functioning of C1q or alter the intended effect of the NDs.

In addition, C1q is involved in the regulation of phagocytosis and cytokine production. C1q has been shown to enhance microglial clearance of apoptotic neurons and neuronal blebs and to suppress the production of pro-inflammatory cytokines.[28] C1q binding on carbon nanotubes can also modulate the phagocytosis and cytokine release of macrophages.[29] Thus,

the binding properties of C1q need to be investigated to understand the clearance of administered NDs.

Here, we investigate the potential of NDs to trigger complement activation through the three complement pathways and the binding properties of NDs with C1q. We used three types of NDs with different physiochemical properties — (i) in their original forms without modification (pristine), (ii) oxidized with surface carboxylic groups, and (iii) functionalized with polyethylene glycol (PEG). Unmodified and oxidized NDs have found various biomedical applications, such as implant coating and drug delivery, respectively.[6,30] Oxidized NDs have also been proposed as a neuroprotective agent against Alzheimer's disease.[10] As PEG is commonly used to evade the mononuclear phagocytic system and increase the circulation time of nanomedicines, PEG-grafted NDs have been developed for selective cancer drug delivery.[31] We used an enzyme immunoassay to test the ND-mediated complement activation in human serum. Surface plasmon resonance (SPR), transmission electron microscopy (TEM), and dynamic light scattering (DLS) were employed to study ND interaction with C1q. Silica nanospheres were studied with TEM to better understand the results of the NDs. We also studied the effect of C1q on the capacity of macrophages to engulf the NDs and to secrete cytokines IL-6 and IL-8. The cytokine IL-6 is involved in cancer signaling, angiogenesis and tumor proliferation through modulation of macrophage polarization, and confers resistance toward some chemotherapeutic agents.[32–34] The pro-inflammatory IL-8 cytokine, on the other hand, is an important mediator in the response of the innate immune system. Modifications on carbon nanotube surface such as oxidation and PEGylation have been shown to ameliorate the activation of IL-6-hepcidin signaling.[35] The IL-6 and IL-8 release induced by the pristine, oxidized, and PEGylated NDs with and without the addition of C1q was measured by immunosorbent assays.

2. Methods

2.1. *Preparation of nanoparticles*

High-pressure high-temperature Syndia® SYP0-0.03 with single crystal NDs of less than 30 nm were purchased from Van Moppes (Geneva, Switzerland). Silica nanospheres (Ludox® SM colloidal silica) were purchased from Sigma-Aldrich and used without any modifications.

2.1.1. *NDs with surface carboxylic groups*

To generate carboxylic groups on the ND surface, 50 mg of NDs were stirred in a H_2SO_4/HNO_3 3:1 mixture (10 mL) for 1 h at 130 °C.[32] The reaction mixture was then diluted with water and centrifuged for 5 min at 8000 rpm. The pellet was collected and washed twice with water, and the residue was dried under vacuum to yield oxidized NDs (ND-COOH).

2.1.2. *PEG-conjugated NDs*

Oxidized NDs were activated by reacting 50 mg of the ND-COOH (as prepared above) with $SOCl_2$ (20 mL) and anhydrous dimethylformamide (1 mL) at 70 °C for 24 h. The NDs were recovered by centrifugation and the pellet was washed with dry tetrahydrofuran (THF). The activated NDs (ND-COCl) were dried under vacuum. The ND-COCl were then mixed with PEG-NH_2 (170 mg, average M_n = 500 g mol^{-1}) and triethylamine (TEA, 1 mL) in 5 mL of anhydrous dimethylformamide (DMF) and stirred for 24 h at 60 °C under a nitrogen atmosphere. The resulting solution was centrifuged for 10 min at 8000 rpm and the pellet was repeatedly washed with methanol (×5) to remove the excess of PEG. A dark residue of PEG-grafted NDs (ND-PEG) was obtained after drying under vacuum.

2.1.3. *NDs characterization*

The ND samples were characterized using thermogravimetric analysis (TGA) and X-ray photoelectron spectroscopy (XPS). Thermogravimetric analysis was performed with Q50 (TA Instruments) under nitrogen flow at a heating rate of 10 °C min^{-1}. X-ray photoelectron spectroscopy was performed with a Kratos Axis Ultra DLD using a high-resolution monochromatic Al Kα line X-ray source at 1486.6 eV. Core level scans were carried out at fix analyzer pass energy of 20 eV and survey spectra were captured at pass energy of 160 eV. To provide an integrated sampling depth of ~15 nm, the photoelectron takeoff angle was kept normal to the surface. An external gold substrate was used as a reference with a binding energy of 84.0 eV for Au 4f. Zeta potential measurements were performed on a Wallis instrument from Cordouan Technologies equipped with a 635 nm laser diode.

2.2. *Complement activation assay*

The ability of NDs to activate complement was measured using the Wieslab complement system screen COMPL300 (Euro Diagnostica), an enzyme immunoassay based on the detection of a neo-antigen expressed during the MAC formation. Normal human serum was incubated with the nanoparticle solutions diluted to 120 µg mL^{-1} in Tris-Buffer-Saline (TBS) (Euromedex) at a ratio of 6:1 (v/v) for 45 min at 37 °C with occasional shaking. The residual functional activities of the classical pathway, the MBL (mannose-binding lectin)-dependent lectin pathway, and the alternative pathway were measured following the kit instructions. IgG-ovalbumin aggregates (immune complexes IC) were prepared and used as a positive control for the activation of the classical complement pathway (final concentration 0.5-1 mg mL^{-1}), as described previously.[33] Zymosan (1 mg mL^{-1}) was used as a positive control for the activation of both the lectin and alternative pathways. Control incubations for complement

activation contained only TBS buffer and were used to define the reference of 100% complement activity of the serum. Three independent experiments in duplicate were performed for each assay. The means of the multiple measurements are presented with the error bars representing the standard deviations of the measurements.

2.3. *Purification of protein C1q and gC1q*

The C1q subunit of C1 was purified from human plasma.[34] The globular head domain gC1q was generated from purified C1q as described previously.[35] Briefly, C1q was treated with collagenase (100 units collagenase from *Clostridium histolyticum* type III (Sigma) per mg of C1q) for 16 h at 37 ºC, and the gC1q obtained was purified by high-pressure gel permeation on a TSK-G3000 SW column (Tosoh Bioscience) equilibrated in 50 mM Tris-HCl, 250 mM NaCl at pH 7.4. As molecules of gC1q tend to aggregate with time, only freshly prepared samples were used in the experiments.

The proteins were dialyzed in TBS and the final concentrations were around 0.8 mg mL^{-1}. The homogeneity of the purified proteins was assessed by sodium dodecyl sulfate-polyacrylamide gel electrophoresis (SDS-PAGE) analysis under reducing and non-reducing conditions and also by TEM.

2.4. *TEM*

For negative staining TEM, ~4 µL of the sample was applied to a mica sheet covered with a film of evaporated carbon. The carbon film was then floated off the mica in ~100 µL of 2% sodium silicotungstate (SST) solution and retrieved onto a 400-mesh copper TEM grid. Imaging was performed on an FEI T12 microscope at 120 kV and recorded on an Orius 832

charged-coupled device, or on an FEI F20 microscope at 200 kV and recorded on an Eagle or a Gatan One View camera.

For cryo-TEM, ~4 µL of the sample was applied to a glow-discharged Quantifoil grid and plunged frozen in liquid ethane using an FEI Vitrobot. Frozen grids were observed on the FEI F20 microscope at 200 kV or on an FEI Polara microscope at 300 kV. Images on the Polara were recorded on an Ultrascan 4000 charge-coupled device.

2.5. *DLS of the NDs in interaction with C1q*

Dynamic light scattering was performed on a Wyatt DynaPro NanoStar with Wyatt disposable 4 µL cuvette. Three measurements of DLS data were collected for 10 acquisitions (5 s for each acquisition) at 25 °C for each experiment. The particles were all modeled as globular.

2.6. *SPR*

Analyses were performed at 25 °C using a Biacore X instrument (GE Healthcare). C1q and human serum albumin (HSA) were diluted to 33 and 25 µg mL^{-1} in 10 mM sodium acetate pH 5.5 and pH 4.0, respectively, and immobilized on a CM5 sensor chip (GE Healthcare) using the amine coupling chemistry in 10 mM Hepes, 150 mM NaCl, 3 mM EDTA, 0.005% surfactant P20, pH 7.4. Binding of the NDs to immobilized C1q (15000-16000 RU) and HSA (7500-8000 RU) was measured at a flow rate of 20 µL min^{-1} with 10 and 20 µg mL^{-1} NDs in TBS, 0.005% surfactant P20, pH 7.4. The specific binding signal was obtained by subtracting the signal recorded over the HSA surface. Injections (10 µL) of 10-20 mM NaOH regenerated the surfaces. For competition experiments, the NDs were pre-incubated with HSA (0.2 mg mL^{-1}) for 10 min at room temperature before injection over the surfaces. Data were analyzed with the BIAevaluation 3.2 software (GE Healthcare).

2.7. *Phagocytosis of NDs by THP-1 macrophages*

THP1 monocytes were cultured in RPMI-1640 medium (Invitrogen) supplemented with 10% (v/v) heat-inactivated fetal calf serum FCS, penicillin (3 U mL^{-1}), and streptomycin (3 µg mL^{-1}). Differentiation into macrophage-like cells was achieved by treatment with 10 nM PMA (Phorbol 12-myristate 13-acetate) for 48 h.[36,37]

Solution of NDs was sonicated for 45 min, diluted to 50 µg mL^{-1} (~10^{12} particles mL^{-1} assuming ND size of 50 nm) in cell medium in the presence of C1q (10 - 100 µg mL^{-1}) when specified and then added to THP1-derived macrophages in culture medium for 24 h at 37 °C and 5% CO_2. After incubation, cells were washed and harvested with 0.25% trypsin/ ethylenediaminetetraacetic acid (EDTA), re-suspended in PBS, and analyzed by flow cytometry. Phagocytosis efficiency was evaluated by cell size and granularity by measuring the light scattering properties (forward scatter (FSC) and side scatter (SSC)). Flow cytometry analyses were performed with MACSQuant VYB cytometer (Miltenyi Biotech, M4D cell imaging platform). For each sample, 10000 events in the analysis gate were collected and the data was treated with the MACSQuantify software.

2.8. *Quantification of Cytokine Release*

Supernatants of THP1 macrophages incubated for 24 h with NDs in the presence or absence of C1q (100 µg mL^{-1}) as mentioned above were collected and then analyzed for IL-6 and IL-8 contents by enzyme-linked immunosorbent assay (ELISA) according to the manufacturer instructions (Covalab).

3. Results

3.1. *Characterization of NDs*

The ND samples were characterized using TGA to verify the presence of functional groups appended on the ND surface. Results are shown in Figure 1 for the oxidized NDs (red curve) and the PEG-grafted NDs (blue curve). The PEG-grafted ND sample undergoes a moderate weight loss (ca. 5%) at around 350 °C, which corresponds to the degradation temperature of the PEG chain (green curve). The oxidized ND sample (red curve) does not show this behavior, further confirming that the weight loss at 350 °C observed for the ND-PEG sample is attributable to the degradation of PEG units.

The chemical composition of the ND samples was analyzed by XPS. As shown in Table 1, the increase in the oxygen content after oxidation of the NDs reflects the introduction of carboxyl-groups at the already oxidized surface of the particles. The oxygen and nitrogen contents further increase (+1.1% and +0.6%, respectively) upon conjugation with the PEG-NH_2 unit. The XPS results are in good agreement with the weight loss observed by TGA that indicates effective PEG functionalization.

Dynamic light scattering analysis of the different NDs indicated that their hydrodynamic diameter in water is in the 40-50 nm range, regardless of the sample (see for example Supplementary Figure 3A). It is to be noted that the hydrodynamic diameter of the same samples increases when in serum, as the mean diameter of the pristine and PEG-NDs is ca.100 nm and that of ND-COOH is ca.110 nm (Supplementary Figure 1).

3.2. *Complement activation capacities of the NDs*

Samples of NDs were incubated with human serum and residual complement activation capacity *via* each of the three complement pathways was measured. Figure 2 shows the results for the non-modified and modified NDs. Within experimental uncertainty, none of the nanoparticles activate the classical or the MBL-dependent lectin pathways for the concentrations tested. However, all the NDs show detectable activity *via* the alternative pathway.

To confirm that the NDs did not interfere with the functioning of the activation assay, we tested the complement activation by adding pristine NDs to the positive control, *i.e.* IC for the test of activation through the classical pathway and to the zymosan for the lectin and alternative pathways. The complement was activated in all these cases as in the case of IC or zymosan alone, indicating that the NDs did not interfere with the assay (data not shown).

3.3. *Binding of NDs to C1q*

3.3.1. *SPR*

The interaction between NDs and C1q was analyzed by SPR. Human serum albumin was used as a reference for non-specific binding. Proteins C1q and HSA were immobilized on the surface of the sensor chip and two concentrations of NDs (10 µg mL^{-1} and 20 µg mL^{-1}) were injected to flow over the surface. As shown in Figure 3A, the raw binding signals show that the three types of NDs bind to both C1q and HSA to a similar extend. Pre-incubation of the NDs with HSA strongly inhibited subsequent binding to HSA but only partially inhibited subsequent binding to C1q (Figure 3B). As we verified that HSA alone did not bind to C1q under these conditions, the results suggest that the binding sites of NDs for HSA and C1q do not completely overlap.

3.3.2. *TEM*

Figure 4A shows transmission electron micrographs of pristine NDs alone. We found well-isolated particles of size ranging from ~30 nm to ~100 nm. Close inspection shows these particles to be aggregates of smaller crystals. Cryo-TEM was also performed on the NDs and no difference in the size distribution of the NDs was observed.

Figure 4B shows the negative staining results of NDs mixed with C1q (0.9 mg mL^{-1} NDs and 50 µg mL^{-1} C1q final concentration). Aggregates of over 10 µm were formed. Electron microscopy of C1q with ND-COOH, ND-PEG showed similar aggregations (Supplementary Figure 2A-B).

Figure 4C shows a higher magnification image of the boxed region in the negatively stained image in Figure 4B. Molecules of C1q can be found around the aggregate. Upon inspection, irregularly shaped particles with straight edges of around 5-20 nm are bound to the globular regions of these C1q molecules (Figure 4D). These bound particles are likely to be ND single crystals in the sample. Figure 4D shows drawings depicting C1q molecules bonded to the particles. From these congregations, we can infer how C1q molecules aggregate the NDs. The C1q molecule consists of six globular domains (gC1q) that can each interact with a ND. Conversely, a ND can attract gC1q domains belonging to multiple C1q molecules. A conglomerate is thus assembled.

As it was difficult to discern details in the aggregates with the accumulation of stain in the negatively stained image (Figure 4B), we performed cryo-TEM on the sample. The ND-C1q

solution was vitrified in liquid ethane. The frozen hydrated sample showed large aggregates as in the negatively stained sample. However, as shown in the example in Figure 4E, we can now visualize individual ND particles of ~50 nm that are connected by structures of very low contrast (white arrow heads in Figure 4E) within the aggregates. While cryo-TEM preserves the sample in its native hydrated state, contrast of protein molecules is low due to their close density to that of buffer and the lack of stain. Examination of the low contrast structures shows clusters of uniform globular particles of ~4 nm, characteristic of C1q, which is recognizable by its set of globular regions (c.f. Figure 4D).

We repeated the experiments with isolated gC1q, enzymatically generated from C1q molecules by digesting the collagen-like regions of the C1q molecules (each C1q molecule yields six gC1q molecules.). We found ND clusters of 50-100 nm decorated with gC1q (0.9 mg mL^{-1} NDs and 60 µg mL^{-1} gC1q final concentrations) but no formation of large aggregates (Figure 4F). These results suggest that the C1q multivalent binding mode is the cause of the ND aggregation observed.

Analogous experiments with ND-COOH and ND-PEG have yielded similar results (see Supplementary Figure 2C-D).

To investigate the generality of agglutination of nanoparticles by C1q, we performed electron microscopy of SiO_2 nanospheres mixed with whole C1q molecules or with isolated gC1q molecules. Compared to NDs, the SiO_2 nanospheres are monodisperse and are easily recognized in electron micrographs. Results are shown in Figure 5. Figure 5A shows the micrographs of C1q and SiO_2 mixed in buffer to yield final concentrations of 25 µg mL^{-1} C1q and 20 mg mL^{-1} SiO_2. Once again, large aggregates of SiO_2 are observed but, compared to

the aggregates formed with NDs, C1q molecules can be distinguished by the different contrast due to the different elemental compositions from SiO_2. Closer inspection clearly shows nanospheres brought together by C1q molecules (Figure 5B). Figure 5C shows the case of gC1q mixed with the SiO_2 nanospheres (final concentration of 45 µg mL^{-1} gC1q and 20 mg mL^{-1} SiO_2) and similar to the case of NDs, nanospheres decorated with isolated gC1q molecules were present but no large aggregates could be observed, providing further evidence that agglutination comes from the multivalent binding of C1q.

3.3.3. *DLS*

To further confirm the aggregation observed by TEM, we performed DLS experiments on ND-PEG with C1q (Supplementary Figure 3). Nanodiamonds alone diluted in TBS up to the concentration used in EM experiments showed an increase of their hydrodynamic diameter up to 90-100 nm whereas C1q showed two main peaks at ~10 nm and ~100 nm, plus a minor peak (< 10 %) at ~1 µm. As NDs and C1q were mixed to final concentrations of 0.9 mg mL^{-1} NDs and 50 µg mL^{-1} C1q mimicking the conditions in the TEM experiments, the peaks under 100 nm diminished and a broad peak between 1 µm and 10 µm became the main peak (~ 90 % intensity), consistent with the TEM observations.

3.4. *Engulfment by macrophages and cellular response*

It has been shown that macrophages readily engulf unmodified NDs.[1,13,14] To investigate the immune impact of the modified NDs, which has not been reported, we analyzed the interaction of ND-COOH and ND-PEG with macrophages and compared the results with that of pristine ND. Uptake of the NDs by macrophages was assessed by flow cytometry and the cellular response of the macrophages was assessed by cytokine assays. The ability of macrophages to internalize NDs was evaluated by measuring cell size and granularity through

their light scattering properties (FSC and SSC). An arbitrary window corresponding to higher granularities was taken as a reference. This window encompassed 1.5% of the cells in the initial measurements before the incubation (Supplementary Figure 4).

The density dot plots of the scattering parameters of the macrophages incubated with NDs are shown in Figure 6. After 24 h incubation time, cell granularity increases slightly for macrophages incubated with ND and ND-PEG, and considerably for macrophages incubated with ND-COOH, which indicates ND accumulation inside the macrophages (Figure 6). Interestingly, when added at a physiological concentration (10 to 100 µg mL^{-1}) to NDs, C1q enhances cell granularity in a dose dependent manner, indicating that C1q increases ND engulfment by macrophages. In the case of pristine ND, significant increase in engulfment was observed with the addition of 100 µg mL^{-1} C1q. Although internalization is not marked for pristine ND and ND-PEG in the presence of low amount of C1q, the percentage of cells lying within the higher granularity window with 100 µg mL^{-1} C1q increases from 4% to 38% and from 3% to 9.5% for pristine ND and ND-PEG, respectively. These results show that binding of C1q to nanoparticles can modify the reaction of macrophages towards the nanoparticles.

To gain further insight into the effect of the NDs on macrophages, supernatants of the phagocytosis assays (without added C1q and with 100 µg mL^{-1} added C1q) were collected and analyzed for their contents in cytokines IL-6 and IL-8.

Our results showed that modified NDs behaved differently from the pristine NDs. As shown in Figure 7, pristine NDs induce a notable release of IL-6 and efficient release of IL-8 by

macrophages. The overall IL-6 increase, however, remains low in comparison to the effect of, for instance, lipopolysaccharide (LPS), a common endotoxin known to boost proinflammatory signaling (Supplementary Figure 5). Surface modification of the NDs significantly reduces the IL-6 and IL-8 cytokine secretions, even for ND-COOH, which were efficiently engulfed (Figure 6). The levels of cytokine production induced by the modified NDs are comparable to those induced by C1q alone (C1q has been reported to stimulate IL-6 and IL-8 in different cell types.[42–46]). The results also show that addition of C1q increases the cytokine production in all the three ND samples for IL-6 and in the two modified ND samples for IL-8. The effect of C1q on pristine ND may be masked by the high level already expressed without the addition of C1q.

4. Discussion

Our enzyme immunoassay results showed that pristine, oxidized and PEGylated NDs did not activate the classical or the MBL-dependent lectin pathway of complement. On the other hand, activities through the alternative pathway were detected. Whereas the classical pathway and the lectin pathways of complement depend on recognition proteins (C1q for the classical pathway, MBL and ficolins for the lectin pathway) that bind pathogens, the alternative pathway maintains a constant low level of activity, which is inhibited by the presence of self-markers. These results are similar to our previous results on other nanoparticles (PEG-functionalized carbon nanotubes and micelles terminated with carboxylic groups), which have also shown no significant activities through the classical or MBL-dependent lectin pathways but detectable activities through the alternative pathway.[22,47] The results suggest that the NDs do not contain motifs that are actively sought after by the activation proteins of the classical or the MBL-dependent lectin pathways. Complement activities, nonetheless, can be triggered by the NDs *via* the alternative pathway.

Despite the lack of activities of the NDs through the classical pathway, results from surface plasmon resonance showed that all ND samples attracted C1q. The similar binding signals for HSA and C1q suggested that the binding of NDs onto C1q was non-specific, consistent with the results that C1 was not activated by the NDs. It has been proposed that the level of complement activation depends on the ligand-binding site within the C1q globular regions. For instance, the gC1q binding site for immunoglobulins, which are strong activators, is located at the opposite side of the binding site for self-derived ligands such as heparin or DNA, which are weak activators.[48] The binding site on gC1q for ND may be close to that for other carbon nanomaterials such as graphene or carbon nanotube, which are also non-activators of the classical pathway.[23]

The observation that C1q binds to PEG-functionalized NDs, similarly to the non-modified NDs, may be a bit surprising since functionalization with PEG is often used to coat nanomaterials so as to evade the immune system. Whereas the TGA and XPS results clearly showed that the surface of the NDs was functionalized, the moderate weight loss shown by TGA at the PEG degradation temperature and the slight increase in the oxygen and nitrogen contents for ND-PEG indicated that functionalization only partially covered the ND surface. Such results are expected as the functionalization depends on defect sites, which are not abundant on ND surface. Since PEG coverage of the surface of the functionalized NDs was only partial and C1q bound readily on non-modified NDs, C1q might have interacted with non-functionalized regions of the modified NDs. This interpretation would be consistent with our recently reported findings that neither C1q nor gC1q bind to carbon nanotubes fully coated with PEG but do bind to carbon nanotubes that are only partially covered with PEG.[33]

Our TEM results showed that C1q agglutinates NDs because of their multivalent binding mode. The six gC1q domains on each C1q molecule are able to bind to distinct ND particles, which in turn can attract gC1q from distinct C1q molecules with their multiple facets. It is interesting to note that C1q binding causes different effects in carbon nanotubes. Whereas C1q binding results in ND aggregation, C1q disaggregates carbon nanotube bundles for nanotubes with diameter over ~10 nm.[22] Rather than attaching to discrete carbon nanotubes, gC1q domains on the same C1q molecules attach to the surface of the same carbon nanotube of large diameter because of the nanotube geometry. The multivalent binding in this case strengthens the attachment of the C1q molecule on the carbon nanotube. The C1q attachment can overcome the attraction among the nanotubes and results in nanotube dispersion (see Supplementary Figure 6).

Our studies further showed that the binding of C1q onto NDs increased their phagocytosis by macrophages. With the addition of 100 $\mu g\ mL^{-1}$ C1q, pristine ND and ND-COOH were very efficiently internalized. Engulfment of ND-PEG also increased but remained moderate with the same amount of added C1q. As TEM results showed that the polyvalent binding mode of C1q agglutinated the NDs studied, the increase in clearance efficiency may be a result of the agglutination. The increase may also have come from the interaction of bound C1q with its partners on the macrophage surface. The higher granularity observed in the case of ND-COOH even without C1q addition may be due to larger particle size, as observed by DLS (Supplementary Figure 1B). The observation could also be due to the surface carboxylate groups; cellular uptake of carbon nanotubes has been shown to increase with surface carboxylate groups, the effect of which is neutralized by PEGylation.[49] Correspondingly, we found that the engulfment of ND-PEG was modest compared to pristine ND and ND-COOH,

even with the addition of 100 μg mL^{-1} C1q. The presence of PEG may have affected the accessibility of the attached C1q for its partners and contributed to the lower clearance efficiency for ND-PEG compared with the cases of pristine ND and ND-COOH.

Results from immunosorbent assays showed that surface functionalization diminished the IL-6 and IL-8 release by macrophages induced by the NDs. These results are in the same line as that for carbon nanotubes, whose toxicity has been shown to decrease with increased functionalization density.[49] We found that addition of C1q prompted increased secretion of the cytokines in all the ND studied except in the case of IL-8 with pristine ND, which might be close to saturation already without the addition of C1q. Whereas IL-6 levels with added C1q remained low and comparable to the secretion induced by C1q alone, IL-8 levels approximately doubled with added C1q in the cases of the modified NDs and were considerably higher than the level attained by C1q without NDs, especially for ND-PEG. Studies with carbon nanotubes have also shown that C1q binding affects cytokine secretions.[29] Thus, even though surface functionalization, such as PEGylation, may shield the nanoparticles from certain immune response, adsorption of proteins, especially proteins with an active role in the immune system, may alter the outcome when the nanoparticles are introduced into the body.

In conclusion, our findings show that C1q agglutinates NDs and C1q binding alters the macrophage response towards the NDs. Attraction of C1q onto the NDs may locally deplete the multifunctional protein C1q and affect the processes that involve C1q. Considering the extensive presence of C1q in the body and its role in diverse physiological and pathological processes, C1q binding onto NDs warrants attention before applying nanomedicines constituting NDs in the clinical setting.

Acknowledgements

We are very grateful to the managers of the IBS platforms, especially the cellular imaging, SPR, DLS, and EM platforms for access to the instruments and for their technical and scientific expertise.

References

(1) Schrand, A. M.; Hens, S. A. C.; Shenderova, O. A. Nanodiamond Particles: Properties and Perspectives for Bioapplications. *Crit. Rev. Solid State Mater. Sci.* **2009**, *34* (1–2), 18–74.

(2) Mochalin, V. N.; Shenderova, O.; Ho, D.; Gogotsi, Y. The Properties and Applications of Nanodiamonds. *Nat. Nanotechnol.* **2012**, *7* (1), 11–23.

(3) Man, H. B.; Ho, D. Nanodiamonds as Platforms for Biology and Medicine. *J. Lab. Autom.* **2013**, *18* (1), 12–18.

(4) Badea, I.; Kaur, R. Nanodiamonds as Novel Nanomaterials for Biomedical Applications: Drug Delivery and Imaging Systems. *Int. J. Nanomedicine* **2013**, 203.

(5) Perevedentseva, E.; Lin, Y.-C.; Jani, M.; Cheng, C.-L. Biomedical Applications of Nanodiamonds in Imaging and Therapy. *Nanomed.* **2013**, *8* (12), 2041–2060.

(6) Chen, Y.-C.; Tsai, C.-Y.; Lee, C.-Y.; Lin, I.-N. In Vitro and in Vivo Evaluation of Ultrananocrystalline Diamond as an Encapsulation Layer for Implantable Microchips. *Acta Biomater.* **2014**, *10* (5), 2187–2199.

(7) Shkurupy, V. A.; Arkhipov, S. A.; Neshchadim, D. V.; Akhramenko, E. S.; Troitskii, A. V. In Vitro Effects of Nanosized Diamond Particles on Macrophages. *Bull. Exp. Biol. Med.* **2015**, *158* (4), 500–503.

(8) Chen, M.; Pierstorff, E. D.; Lam, R.; Li, S.-Y.; Huang, H.; Osawa, E. *et al.* Nanodiamond-Mediated Delivery of Water-Insoluble Therapeutics. *ACS Nano* **2009**, *3* (7), 2016–2022.

(9) Wang, Z.; Tian, Z.; Dong, Y.; Li, L.; Tian, L.; Li, Y. *et al*. Nanodiamond-Conjugated Transferrin as Chemotherapeutic Drug Delivery. *Diam. Relat. Mater.* **2015**, *58*, 84–93.

(10) Alawdi, S. H.; El-Denshary, E. S.; Safar, M. M.; Eidi, H.; David, M.-O.; Abdel-Wahhab, M. A. Neuroprotective Effect of Nanodiamond in Alzheimer's Disease Rat Model: A Pivotal Role for Modulating NF-KB and STAT3 Signaling. *Mol. Neurobiol.* **2017**, *54* (3), 1906–1918.

(11) Haziza, S.; Mohan, N.; Loe-Mie, Y.; Lepagnol-Bestel, A.-M.; Massou, S.; Adam, M.-P. *et al.* Fluorescent Nanodiamond Tracking Reveals Intraneuronal Transport Abnormalities Induced by Brain-Disease-Related Genetic Risk Factors. *Nat. Nanotechnol.* **2017**, *12* (4), 322–328.

(12) Kurantowicz, N.; Strojny, B.; Sawosz, E.; Jaworski, S.; Kutwin, M.; Grodzik, M. *et al*. Biodistribution of a High Dose of Diamond, Graphite, and Graphene Oxide Nanoparticles After Multiple Intraperitoneal Injections in Rats. *Nanoscale Res. Lett.* **2015**, *10* (1), 398.

(13) Yuan, Y.; Wang, X.; Jia, G.; Liu, J.-H.; Wang, T.; Gu, Y. *et al*. Pulmonary Toxicity and Translocation of Nanodiamonds in Mice. *Diam. Relat. Mater.* **2010**, *19* (4), 291–299.

(14) Thomas, V.; Halloran, B. A.; Ambalavanan, N.; Catledge, S. A.; Vohra, Y. K. In Vitro Studies on the Effect of Particle Size on Macrophage Responses to Nanodiamond Wear Debris. *Acta Biomater.* **2012**, *8* (5), 1939–1947.

(15) Vaijayanthimala, V.; Cheng, P.-Y.; Yeh, S.-H.; Liu, K.-K.; Hsiao, C.-H.; Chao, J.-I. *et al*. The Long-Term Stability and Biocompatibility of Fluorescent Nanodiamond as an in Vivo Contrast Agent. *Biomaterials* **2012**, *33* (31), 7794–7802.

(16) Zhao, L.; Xu, Y.-H.; Akasaka, T.; Abe, S.; Komatsu, N.; Watari, F. *et al*. Polyglycerol-Coated Nanodiamond as a Macrophage-Evading Platform for Selective Drug Delivery in Cancer Cells. *Biomaterials* **2014**, *35* (20), 5393–5406.

(17) Baron, A. V.; Puzyr, A. P.; Baron, I. I.; Bondar, V. S. Effects of Modified Detonation Nanodiamonds on the Biochemical Composition of Human Blood. *Bull. Exp. Biol. Med.* **2013**, *154* (6), 781–784.

(18) Baron, A. V.; Osipov, N. V.; Olkhovskiy, I. A.; Puzyr, A. P.; Bondar, V. S. Binding the Immunoglobulins of Human Serum by Nanodiamonds. *Dokl. Biochem. Biophys.* **2014**, *457* (1), 158–159.

(19) Moghimi, S. M.; Andersen, A. J.; Ahmadvand, D.; Wibroe, P. P.; Andresen, T. L.; Hunter, A. C. Material Properties in Complement Activation. *Adv. Drug Deliv. Rev.* **2011**, *63* (12), 1000–1007.

(20) Strang, C. J.; Siegel, R. C.; Phillips, M. L.; Poon, P. H.; Schumaker, V. N. Ultrastructure of the First Component of Human Complement: Electron Microscopy of the Crosslinked Complex. *Proc. Natl. Acad. Sci. U. S. A.* **1982**, *79* (2), 586–590.

(21) Gaboriaud, C.; Juanhuix, J.; Gruez, A.; Lacroix, M.; Darnault, C.; Pignol, D. *et al*. The Crystal Structure of the Globular Head of Complement Protein C1q Provides a Basis for Its Versatile Recognition Properties. *J. Biol. Chem.* **2003**, *278* (47), 46974–46982.

(22) Saint-Cricq, M.; Carrete, J.; Gaboriaud, C.; Gravel, E.; Doris, E.; Thielens, N. *et al*. Human Immune Protein C1q Selectively Disaggregates Carbon Nanotubes. *Nano Lett.* **2017**, *17* (6), 3409–3415.

(23) Ling, W. L.; Biro, A.; Bally, I.; Tacnet, P.; Deniaud, A.; Doris, E. *et al*. Proteins of the Innate Immune System Crystallize on Carbon Nanotubes but Are Not Activated. *ACS Nano* **2011**, *5* (2), 730–737.

(24) Nayak, A.; Ferluga, J.; Tsolaki, A. G.; Kishore, U. The Non-Classical Functions of the Classical Complement Pathway Recognition Subcomponent C1q. *Immunol. Lett.* **2010**, *131* (2), 139–150.

(25) Ghebrehiwet, B.; Hosszu, K.; Valentino, A.; Peerschke, E. I. B. The C1q Family of Proteins: Insights into the Emerging Non-Traditional Functions. *Front. Immunol.* **2012**, *3*.

(26) Hong, S.; Beja-Glasser, V. F.; Nfonoyim, B. M.; Frouin, A.; Li, S.; Ramakrishnan, S. *et al*. Complement and Microglia Mediate Early Synapse Loss in Alzheimer Mouse Models. *Science* **2016**, *352* (6286), 712–716.

(27) Lui, H.; Zhang, J.; Makinson, S. R.; Cahill, M. K.; Kelley, K. W.; Huang, H.-Y. *et al*. Progranulin Deficiency Promotes Circuit-Specific Synaptic Pruning by Microglia via Complement Activation. *Cell* **2016**, *165* (4), 921–935.

(28) Fraser, D. A.; Pisalyaput, K.; Tenner, A. J. C1q Enhances Microglial Clearance of Apoptotic Neurons and Neuronal Blebs, and Modulates Subsequent Inflammatory Cytokine Production. *J. Neurochem.* **2010**, *112* (3), 733–743.

(29) Pondman, K. M.; Sobik, M.; Nayak, A.; Tsolaki, A. G.; Jäkel, A.; Flahaut, E. *et al*. Complement Activation by Carbon Nanotubes and Its Influence on the

Phagocytosis and Cytokine Response by Macrophages. *Nanomedicine Nanotechnol. Biol. Med.* **2014**, *10* (6), 1287–1299.

(30) Lim, D. G.; Kim, K. H.; Kang, E.; Lim, S. H.; Ricci, J.; Sung, S. K. *et al*. Comprehensive evaluation of carboxylated nanodiamond as a topical drug delivery system https://www.dovepress.com/comprehensive-evaluation-of-carboxylated-nanodiamond-as-a-topical-drug-peer-reviewed-fulltext-article-IJN (accessed Sep 12, 2017).

(31) Wang, D.; Tong, Y.; Li, Y.; Tian, Z.; Cao, R.; Yang, B. PEGylated Nanodiamond for Chemotherapeutic Drug Delivery. *Diam. Relat. Mater.* **2013**, *36*, 26–34.

(32) Wei, L.-H.; Kuo, M.-L.; Chen, C.-A.; Chou, C.-H.; Lai, K.-B.; Lee, C.-N. *et al*. Interleukin-6 Promotes Cervical Tumor Growth by VEGF-Dependent Angiogenesis via a STAT3 Pathway. *Oncogene* **2003**, *22* (10), 1517–1527.

(33) Natarajan, K.; Singh, S.; Burke, T. R.; Grunberger, D.; Aggarwal, B. B. Caffeic Acid Phenethyl Ester Is a Potent and Specific Inhibitor of Activation of Nuclear Transcription Factor NF-Kappa B. *Proc. Natl. Acad. Sci. U. S. A.* **1996**, *93* (17), 9090–9095.

(34) Roca, H.; Varsos, Z. S.; Sud, S.; Craig, M. J.; Ying, C.; Pienta, K. J. CCL2 and Interleukin-6 Promote Survival of Human CD11b(+) Peripheral Blood Mononuclear Cells and Induce M2-Type Macrophage Polarization. *J. Biol. Chem.* **2009**, *284* (49), 34342–34354.

(35) Ma, J.; Li, R.; Liu, Y.; Qu, G.; Liu, J.; Guo, W.; *et al*. Carbon Nanotubes Disrupt Iron Homeostasis and Induce Anemia of Inflammation through Inflammatory Pathway as a Secondary Effect Distant to Their Portal-of-Entry. *Small* **2017**, *13* (15), n/a-n/a.

(36) Krueger, A.; Lang, D. Functionality Is Key: Recent Progress in the Surface Modification of Nanodiamond. *Adv. Funct. Mater.* **2012**, *22* (5), 890–906.

(37) Belime, A.; Gravel, E.; Brenet, S.; Ancelet, S.; Caneiro, C.; Hou, Y. *et al*. Mode of PEG Coverage on Carbon Nanotubes Affects Binding of Innate Immune Protein C1q. *J. Phys. Chem. B* **2017**.

(38) Arlaud, G. J.; Sim, R. B.; Duplaa, A.-M.; Colomb, M. G. Differential Elution of Clq, Cl[Combining Macron]r and Cl[Combining Macron]s from Human CT Bound to Immune Aggregates. Use in the Rapid Purification of Cl[Combining Macron] Sub-Components. *Mol. Immunol.* **1979**, *16* (7), 445–450.

(39) Tacnet-Delorme, P.; Chevallier, S.; Arlaud, G. J. β-Amyloid Fibrils Activate the C1 Complex of Complement Under Physiological Conditions: Evidence for a Binding Site for Aβ on the C1q Globular Regions. *J Immunol* **2001**, *167* (11), 6374–6381.

(40) Daigneault, M.; Preston, J. A.; Marriott, H. M.; Whyte, M. K. B.; Dockrell, D. H. The Identification of Markers of Macrophage Differentiation in PMA-Stimulated THP-1 Cells and Monocyte-Derived Macrophages. *PLOS ONE* **2010**, *5* (1), e8668.

(41) Verneret, M.; Tacnet-Delorme, P.; Osman, R.; Awad, R.; Grichine, A.; Kleman, J.-P. *et al*. Relative Contribution of C1q and Apoptotic Cell-Surface Calreticulin to Macrophage Phagocytosis. *J. Innate Immun.* **2014**, *6* (4), 426–434.

(42) Xiao, S.; Xu, C.; Jarvis, J. N. C1q-Bearing Immune Complexes Induce IL-8 Secretion in Human Umbilical Vein Endothelial Cells (HUVEC) through Protein Tyrosine Kinase- and Mitogen-Activated Protein Kinase-Dependent Mechanisms: Evidence That the 126 KD Phagocytic C1q Receptor Mediates Immune Complex Activation of HUVEC. *Clin. Exp. Immunol.* **2001**, *125* (3), 360–367.

(43) Khalkhali-Ellis, Z.; Bulla, G. A.; Schlesinger, L. S.; Kirschmann, D. A.; Moore, T. L.; Hendrix, M. J. C. C1q-Containing Immune Complexes Purified from Sera of Juvenile Rheumatoid Arthritis Patients Mediate IL-8 Production by Human Synoviocytes: Role of C1q Receptors. *J. Immunol.* **1999**, *163* (8), 4612–4620.

(44) Fox, S.; Ryan, K. A.; Berger, A. H.; Petro, K.; Das, S.; Crowe, S. E. *et al*. The Role of C1q in Recognition of Apoptotic Epithelial Cells and Inflammatory Cytokine Production by Phagocytes during Helicobacter Pylori Infection. *J. Inflamm.-Lond.* **2015**, *12*.

(45) Ghebrehiwet, B.; Tantral, L.; Titmus, M. A.; Panessa-Warren, B. J.; Tortora, G. T.; Wong, S. S. *et al*. The Exosporium of B.Cereus Contains a Binding Site for GC1qR/P33: Implication in Spore Attachment and/or Entry. In *Current Topics in Innate Immunity*; Lambris, J. D., Ed.; Springer-Verlag Berlin: Berlin, 2007; Vol. 598, pp 181–197.

(46) Berg, R. H. van den; Faber-Krol, M. C.; Sim, R. B.; Daha, M. R. The First Subcomponent of Complement, C1q, Triggers the Production of IL-8, IL-6, and Monocyte Chemoattractant Peptide-1 by Human Umbilical Vein Endothelial Cells. *J. Immunol.* **1998**, *161* (12), 6924–6930.

(47) Thielens, N. M.; Belime, A.; Gravel, E.; Ancelet, S.; Caneiro, C.; Doris, E. *et al*. Impact of the Surface Charge of Polydiacetylene Micelles on Their Interaction with Human Innate Immune Protein C1q and the Complement System. *Int. J. Pharm.* **2018**, *536* (1), 434–439.

(48) Garlatti, V.; Chouquet, A.; Lunardi, T.; Vives, R.; Paidassi, H.; Lortat-Jacob, H. *et al*. Cutting Edge: C1q Binds Deoxyribose and Heparan Sulfate through Neighboring Sites of Its Recognition Domain. *J. Immunol.* **2010**, *185* (2), 808–812.

(49) Singh, R. P.; Das, M.; Thakare, V.; Jain, S. Functionalization Density Dependent Toxicity of Oxidized Multiwalled Carbon Nanotubes in a Murine Macrophage Cell Line. *Chem. Res. Toxicol.* **2012**, *25* (10), 2127–2137.

Figure Legends

Figure 1. **Thermogravimetric analysis of functionalized nanodiamonds (NDs).** Nanodiamonds functionalized with PEG showed weight loss at ~350 °C, corresponding to the degradation temperature of PEG.

Figure 2. **Complement activation assays of NDs.** Normal human serum (NHS) was incubated for 45 min at 37 °C with the ND solutions at 120 µg mL^{-1} and the residual functional activities of the classical pathway, the MBL-dependent lectin pathway, and the alternative pathway of complement were measured. IgG-ovalbumin immune complexes (IC) were used as a positive control for complement activation via the classical pathway, and zymosan (Zym) for the lectin and alternative pathways. Measurement of reference NHS complement activity was performed in the buffer (TBS) without NDs. Results are expressed in percentage (%) of NHS activity (mean +/- standard deviation of three independent experiments performed in duplicate).

Figure 3. **Surface plasmon resonance analysis of the interaction of NDs with C1q and human serum albumin (HSA).** (A) The three types of NDs at two indicated concentrations were injected over immobilized C1q and HSA, which was used as a reference for non-specific binding. The binding signals obtained over each protein and the specific binding signal obtained after subtraction of HSA are shown. (B) Nanodiamonds (10 µg mL^{-1}) were pre-incubated with HSA (200 µg mL^{-1}) or buffer (negative control) before injection over immobilized C1q and HSA. Results are representative of two independent experiments performed on different sensor chips.

Figure 4. **Transmission electron micrographs of non-modified NDs and their interactions with C1q and gC1q.** (A) Nanodiamond particles show size distribution of ~30-100 nm. (B) Negatively stained sample of NDs mixed with C1q shows aggregates of over 10 µm. (C) Higher magnification image of boxed region in (B) showing molecules of C1q around the large ND-C1q aggregate. (D) Close-ups of some negatively stained C1q molecules with bound NDs and their schematic diagrams showing the mechanism of aggregation. Individual ND may bind multiple globular domains of one or more C1q molecules. (E) Cryo-electron micrograph of the same sample as in (B) with no heavy metal staining shows that the large aggregates are not solidly packed but consist of separated ND particles of ~50 nm. Although the contrast is low in the unstained specimen, molecules of C1q (white arrowheads) can be recognized by clusters of their globular domains (gC1q) in the space in between the ND particles. (F) Interaction of the isolated gC1q molecules with NDs (negative staining). White arrowheads point to examples of bound gC1q on ND particles.

Figure 5. **Transmission electron micrographs of silica nanospheres interacting with C1q and isolated gC1q.** (A) Sample of silica nanospheres mixed with C1q shows large aggregates of nanospheres. The globular domains of the C1q molecules can be recognized among the nanosphere aggregates as bright regular dots. (B) Higher magnification images and schematic representations of small clusters of nanospheres linked by C1q molecules. (C) Interaction of the isolated gC1q with the nanospheres. Nanospheres are decorated with gC1q but no large aggregations are observed. The same scale applies to (A) and (C).

Figure 6. **Nanodiamond uptake by THP1 macrophages.** Density dot plots of forward scattering (FSC) and side scattering (SSC) parameters (arbitrary values) of pristine ND, ND-COOH and ND-PEG added to THP1 macrophages with and without addition of C1q.

Percentage of events in gate corresponding to higher granularities that lie in the boxed region is indicated in each case. Results are representative of three independent experiments.

Figure 7. **Cytokine secretion by THP1 macrophages incubated with NDs with and without C1q.** Supernatants of THP1 macrophages incubated with pristine ND, ND-COOH or ND-PEG, in the presence or absence of C1q, were collected at 24 h and quantified for their content of IL-6 and IL-8 by ELISA. The mean of three measurements is presented in each case with the error bars representing the standard deviations of the measurements.

Table Legend

Table 1. **Element contents (%) of the three ND samples based on the XPS analysis.**

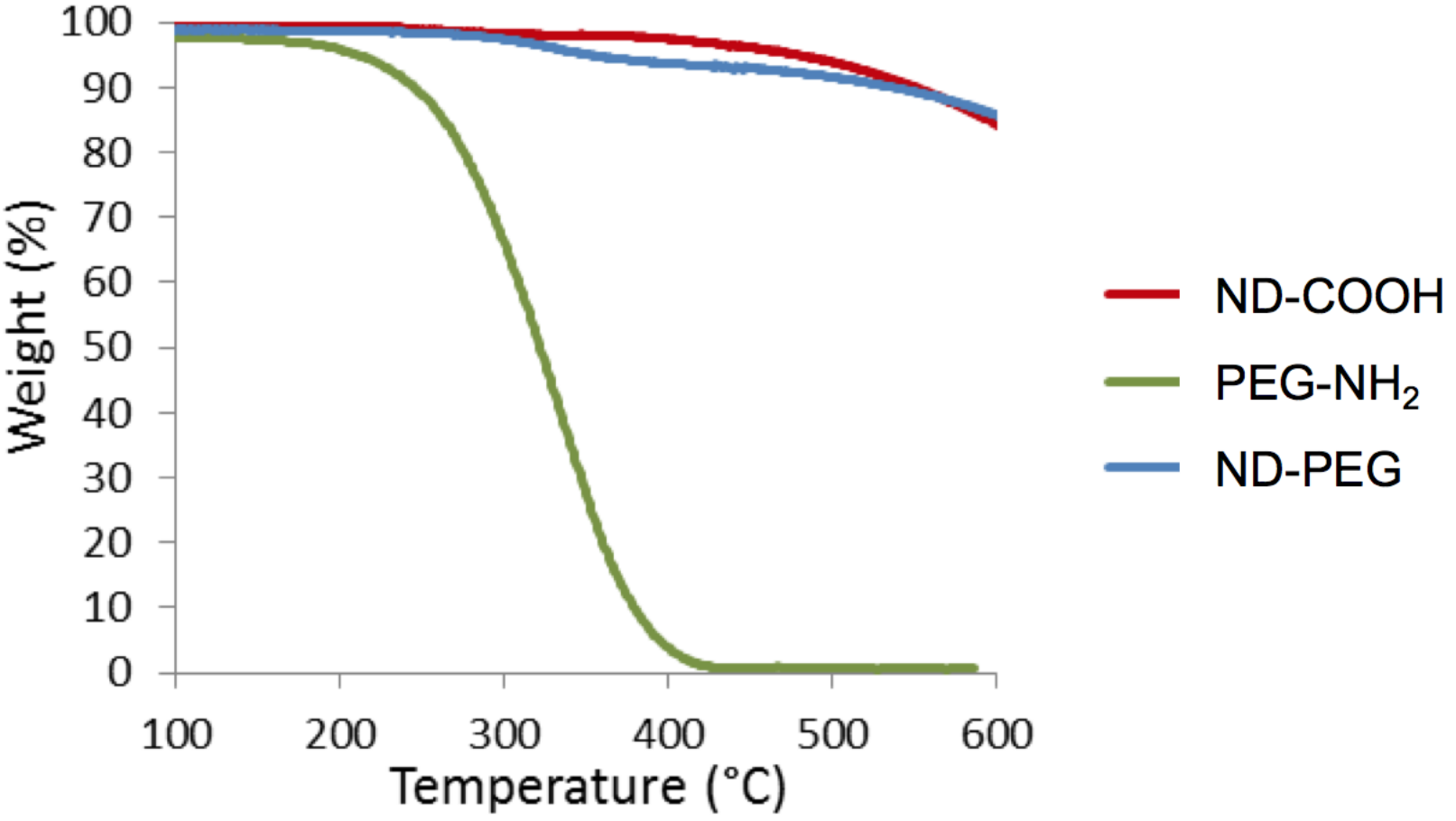
100
90
80
70
60
50
40
30
20
10
0
Weight (%)
100
200
300
400
500
600
Temperature (°C)
ND-COOH
PEG-NH2
ND-PEG

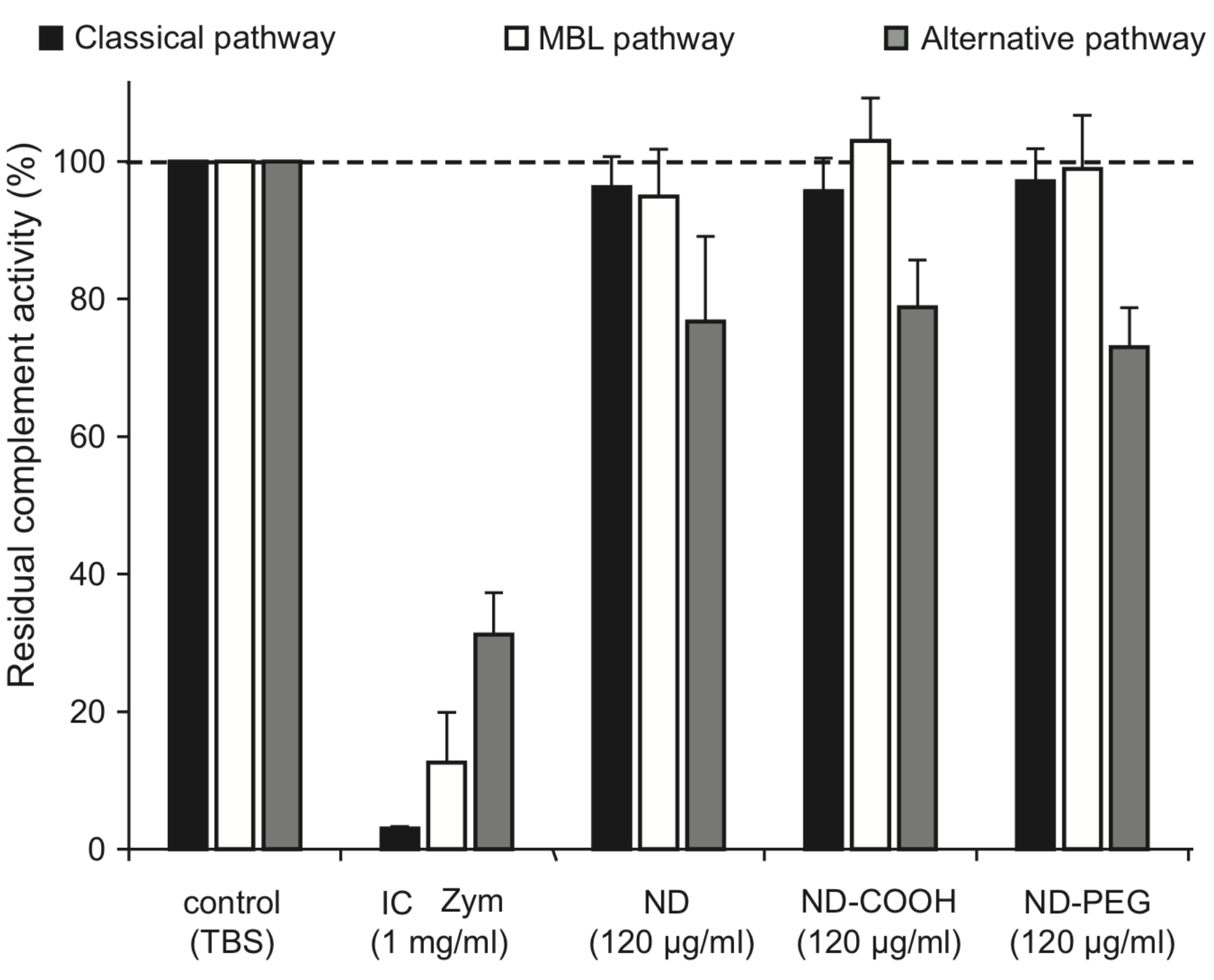
Classical pathway
MBL pathway
Alternative pathway
Residual complement activity (%)
100
80
60
40
20
0
control (TBS)
IC
Zym (1 mg/ml)
ND (120 µg/ml)
ND-COOH (120 µg/ml)
ND-PEG (120 µg/ml)

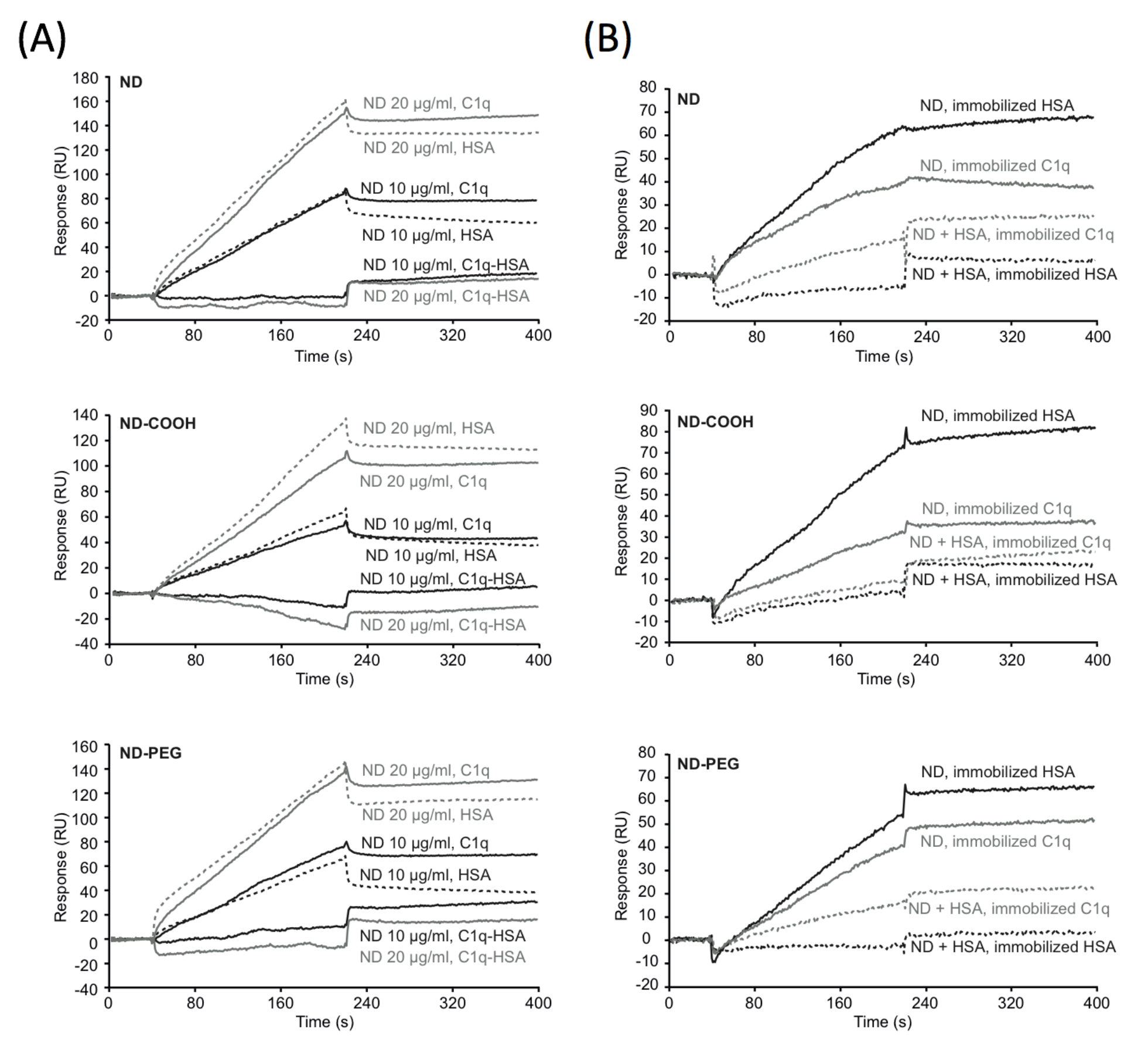
(A)
(B)
ND
ND 20 µg/ml, C1q
ND 20 µg/ml, HSA
ND 10 µg/ml, C1q
ND 10 µg/ml, HSA
ND 10 µg/ml, C1q-HSA
ND 20 µg/ml, C1q-HSA
Response (RU)
Time (s)
ND, immobilized HSA
ND, immobilized C1q
ND + HSA, immobilized C1q
ND + HSA, immobilized HSA
ND-COOH
ND-PEG

(A)

200 nm

(B)

1 µm

(C)

200 nm

(D)

(E)

100 nm

(F)

200 nm

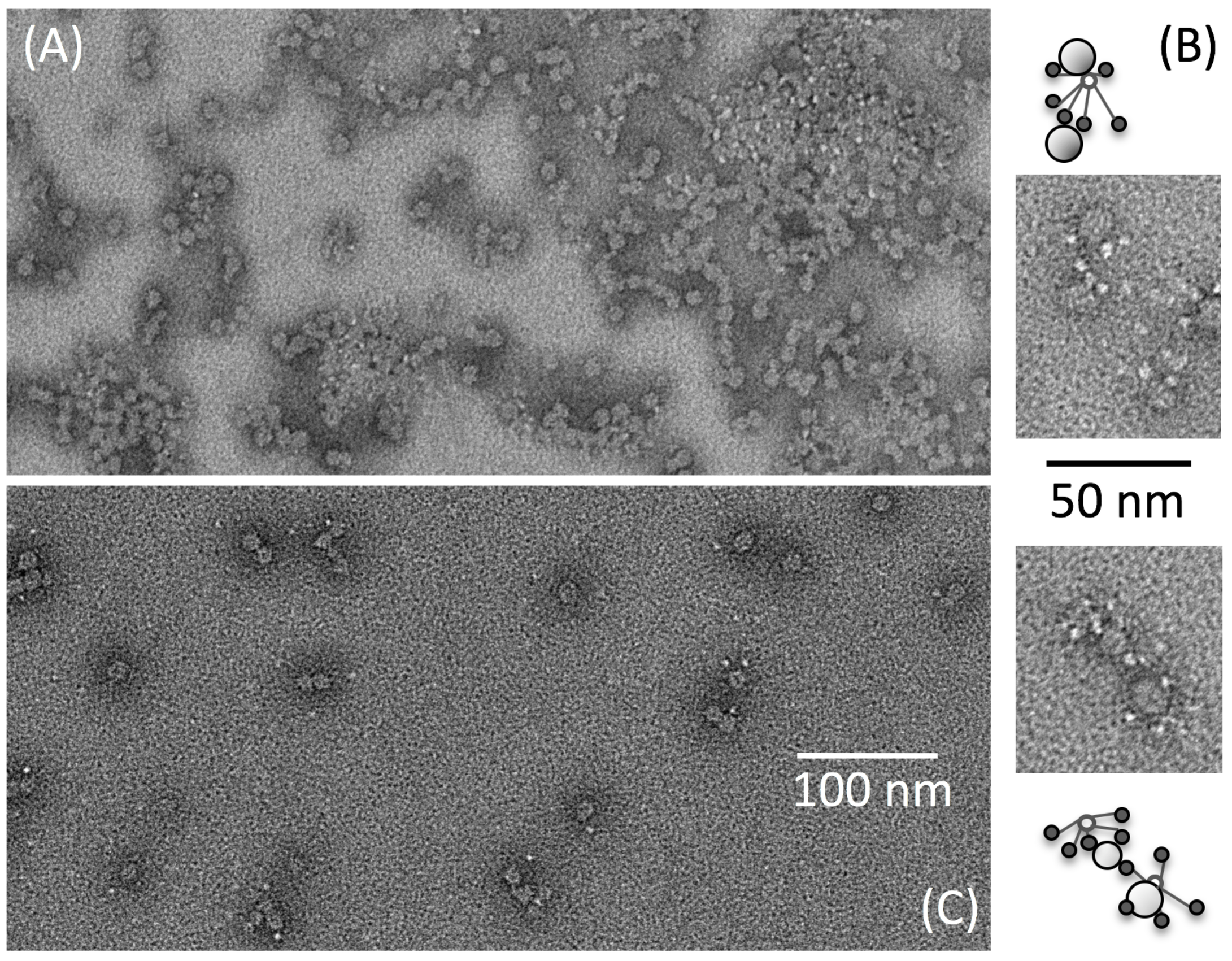
(A)
(B)
50 nm
100 nm
(C)

	with no added C1q	+C1q 10 µg/ml	+C1q 100 µg/ml
ND	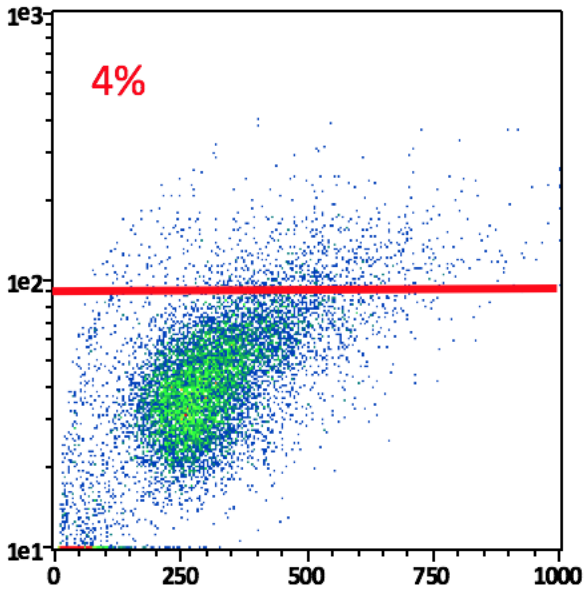	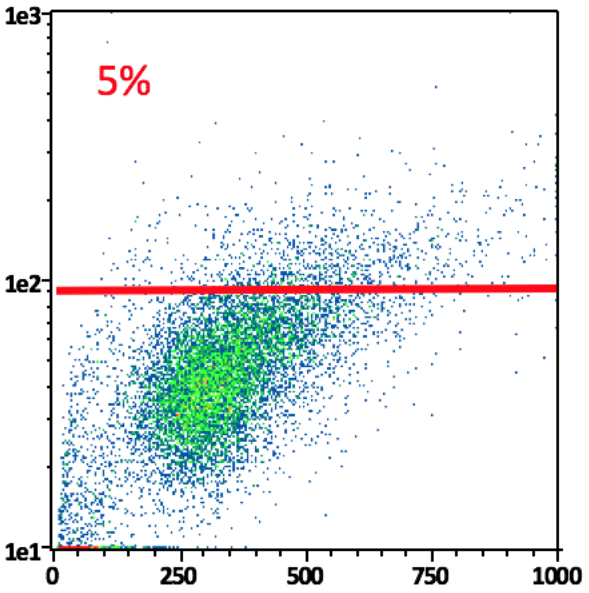	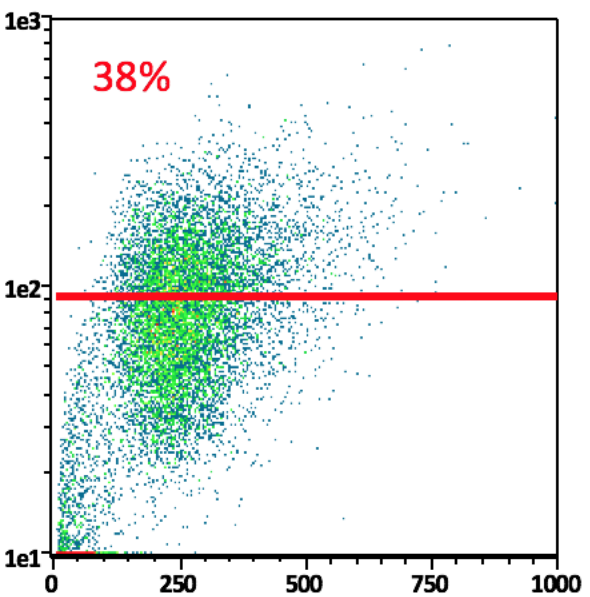
ND-COOH	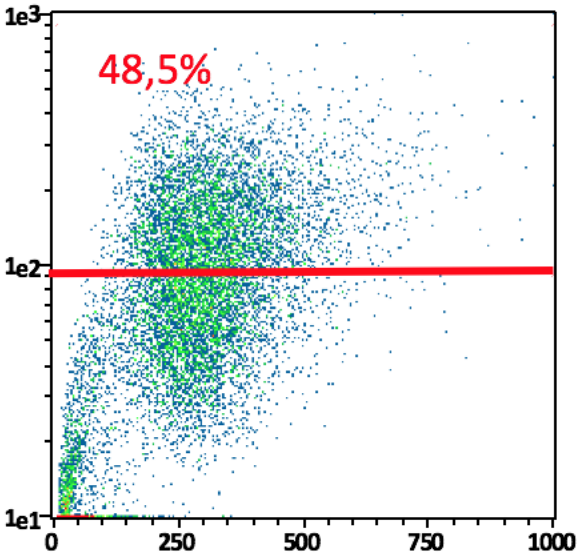	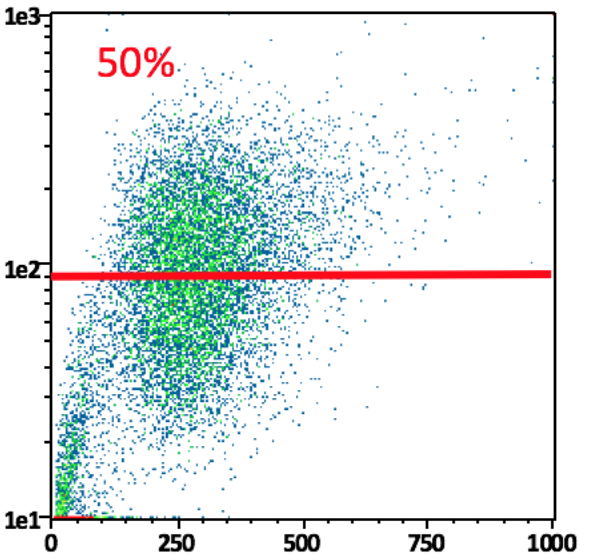	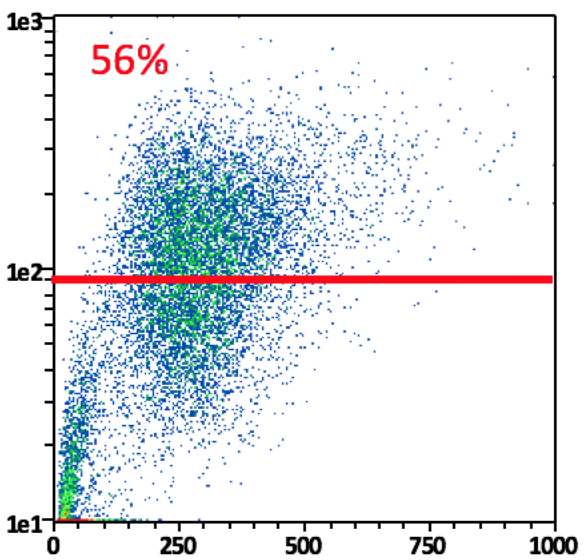
ND-PEG	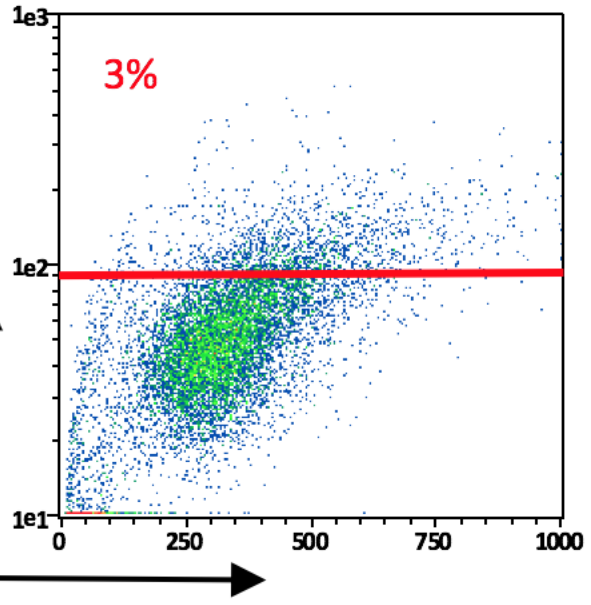	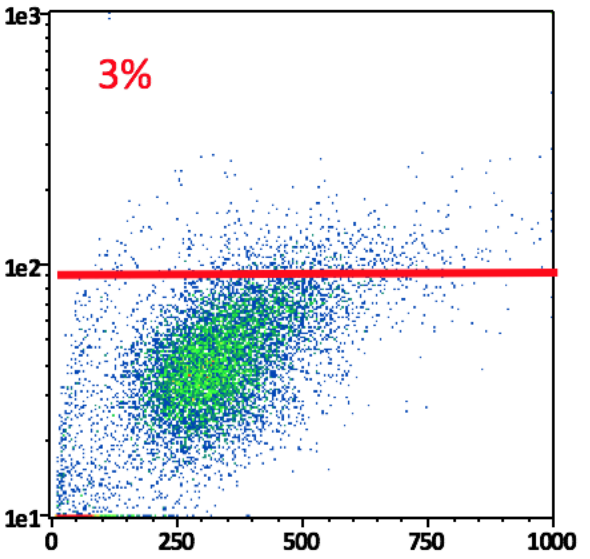	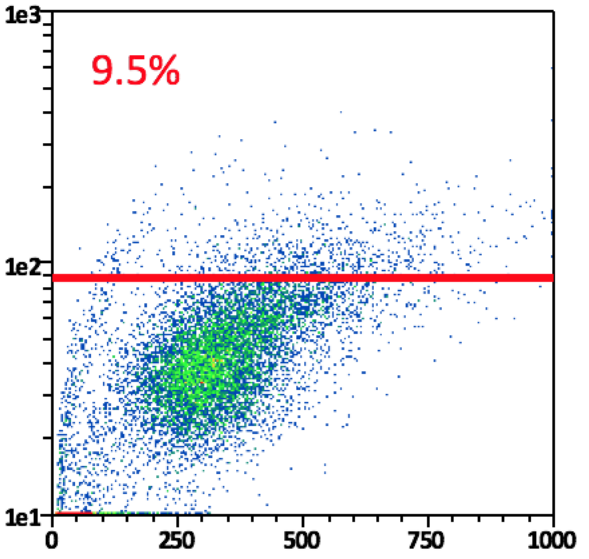

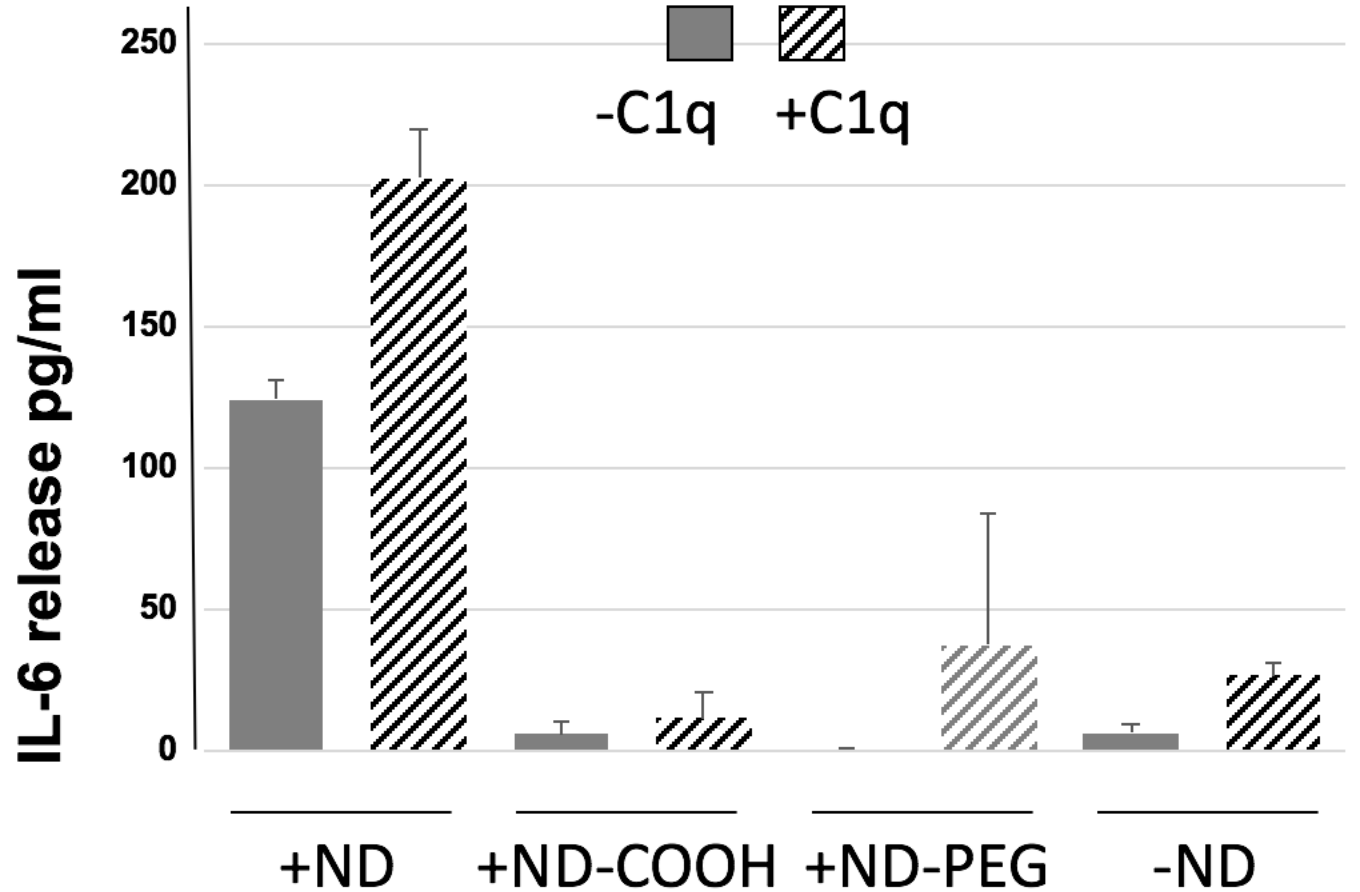
-C1q
+C1q
IL-6 release pg/ml
250
200
150
100
50
0
+ND
+ND-COOH
+ND-PEG
-ND

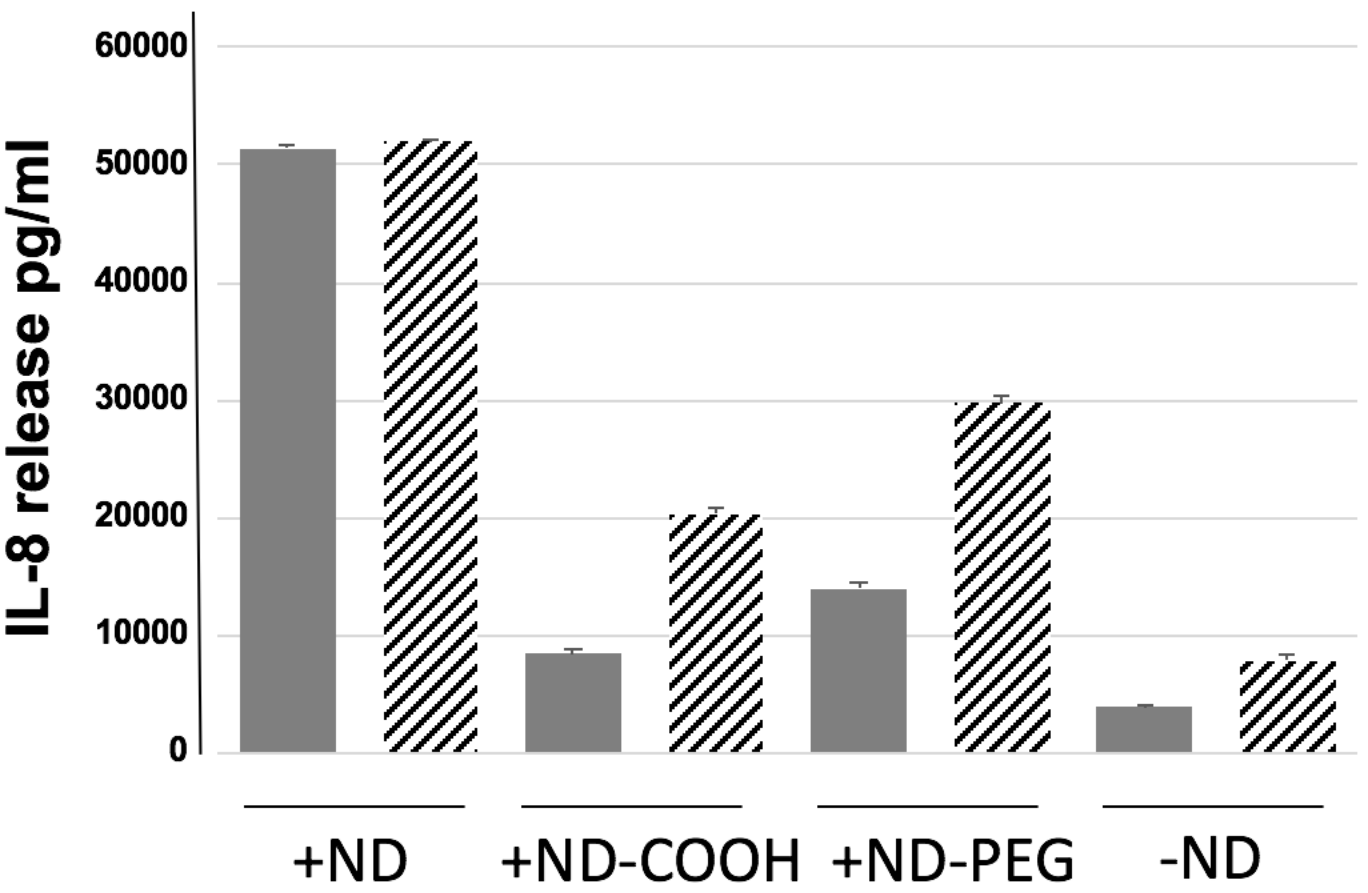
IL-8 release pg/ml
60000
50000
40000
30000
20000
10000
0
+ND
+ND-COOH
+ND-PEG
-ND

Sample	C1s	O1s	N1s
ND	91.8	8.2	--
ND-COOH	89.9	10.1	--
ND-PEG	88.2	11.2	0.6

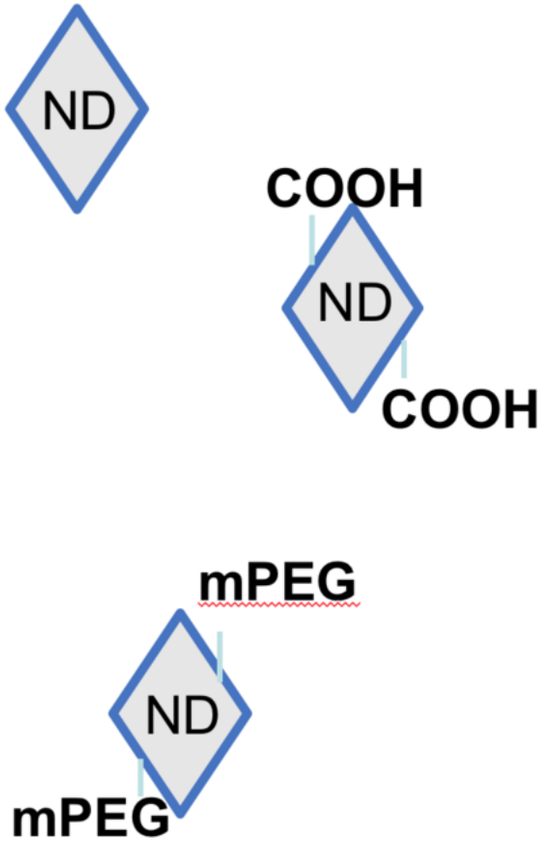
ND
COOH
ND
COOH
mPEG
ND
mPEG

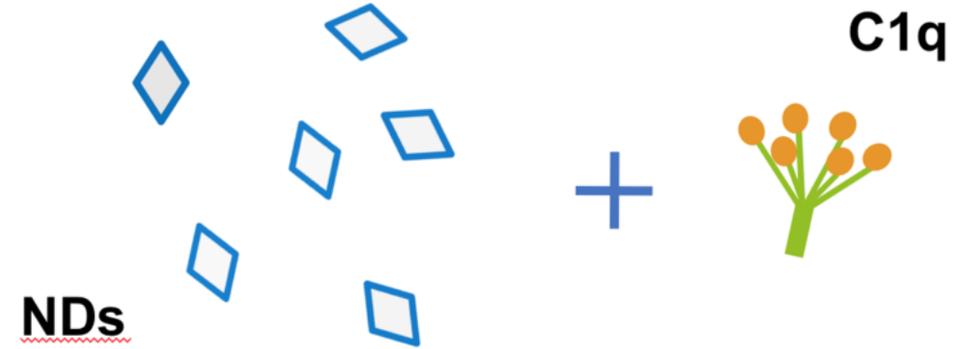
C1q
NDs

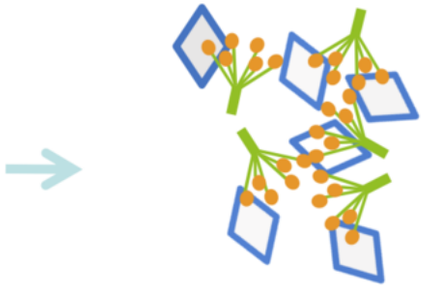
ND-C1q aggregates

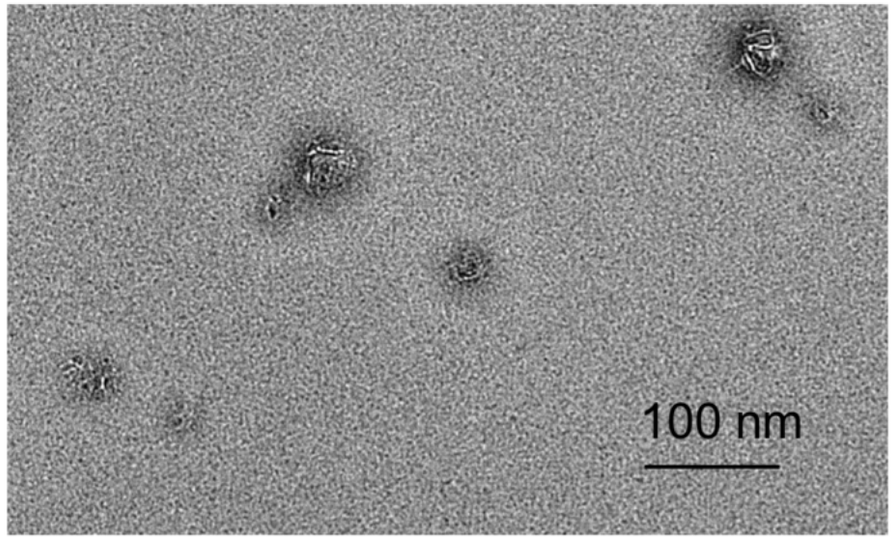
100 nm

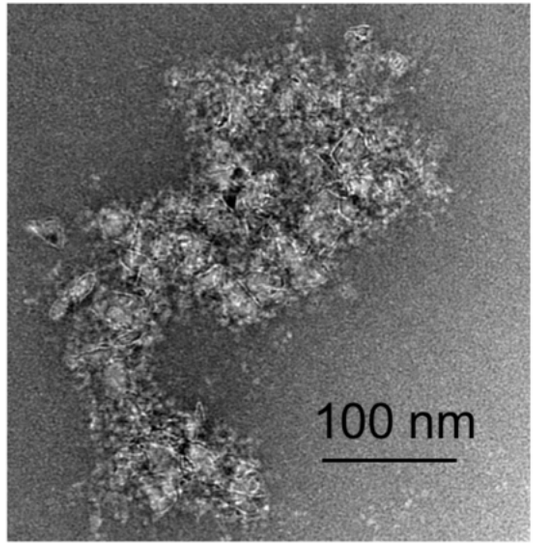
100 nm